Tension distribution analysis of Dual-Tendon routings for Exo-Glove II

Byungchul Kim, Useok Jeong, and Kyu-Jin Cho

This supplementary document explains a method to calculate the tension distribution of a system with dual-tendon routing. Here, the tension distributions of seven tendon routings (i.e., TR1 - TR7 introduced in the main text) were derived.

A. Friction modeling of a tendon

Basically, the friction applied on the tendon can be derived using a capstan equation [1]. This equation is used to calculate the friction that occurs when the tendon routing is curved. The relation between the input tension (T_{in} in Fig. 1(a)) and the output tension (T_{out} in Fig. 1(a)) is described as

$$T_{out} = T_{in} e^{-\mu\theta\delta} \tag{1}$$

where, θ is curvature angle and δ is the sign of relative velocity of the tendon.

The relationship between the input tension and the output tension varies based on whether the tendon moves along a non-rotating object, such as a Teflon tube, or if it moves along a rotating object, such as a bearing. When the tendon passes a fixed curvature, such as a Teflon tube, the friction of the tendon can be simply defined as

$$\begin{aligned} f_{static} &\leq T_{in}(1 - e^{-\mu_s\theta\delta}) \\ f_{kinetic} &= T_{in}(1 - e^{-\mu_k\theta\delta}) \end{aligned} \tag{2}$$

where, f_{static} is the friction when the tendon does not move and $f_{kinetic}$ is the friction when the tendon moves, respectively.

On the other hand, when the tendon passes by the rotating curvature, we should consider the friction between the tendon and the bearing cover (f in the Fig. 1(b)) and the friction inside the bearing (g in the Fig. 1(b)). Since the mass of the bearing is negligible, we can assume the f and g should be equal, because of the force equilibrium; when f and g are not equal, the rotational acceleration becomes infinite. Since the outer part of the bearing rotates against the inner side of the bearing, g can be figured out using the rotational friction coefficient (μ_r) as

$$f_{rotary} = g_{rotary} = T_{in}(1 - e^{-\mu_r\delta\theta}). \tag{3}$$

One problem of the friction equations given above is that it is difficult to estimate the static friction; we can only know that the friction is smaller than the maximum static friction. For this reason, we assumed that the tendon elongates toward the direction where a large tension is applied. For instance, in a case where one end of the tendon is tied and the other is pulled, the tendon will not make a motion. However, by assuming the tendon elongation, we estimated the friction as a kinetic friction. The kinetic friction coefficient of the Teflon tube and the rotational friction coefficient of the bearing used in the modelling are 0.18 and 0.001, respectively [2]. Since the process of deriving the tension of each segment begins with finding the direction in which the tendon moves (δ in above equations), details of deriving tension distribution are explained in the following segments by considering the kinematic conditions of the tendon.

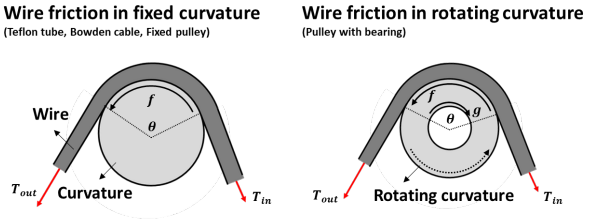

Fig. 1. **Schematic to derive the tendon friction at a curvature**
Since the friction depends on the relative distance between objects, the friction is defined by whether the tendon is moving along a fixed curvature or a rotating curvature.

B. Tension distribution of tendon routing 1

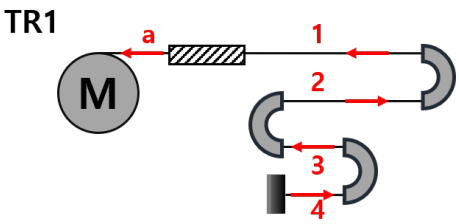

Fig. 2. **Schematic of tendon routing 1**
Tendon routing 1 (TR1) schematic to derive the tension distribution.

TABLE I
TENSION DISTRIBUTION OF TENDON ROUTING 1

TR1	T_M	T_1	T_2	T_3	T_4
	1	0.32	0.18	0.10	0.06
Ratio	-	48(%)	27(%)	16(%)	9(%)

In TR1 (Fig. 2), one side of the tendon is fixed at the end-effector, while the other side of the tendon is fixed at the motor. In this case, the tension distribution can be obtained because the pulling direction of the tendon is straightforward.

Here, when the motor pulls the tendon, the tendon passes from segment 4 to segment 1 and finally it moves to segment a. Therefore, the force equations of the tension can be described as

$$\begin{aligned} T_M &= T_a \\ T_3 - T_4 &= T_3(1 - e^{-\mu_t \pi}) \\ T_2 - T_3 &= T_2(1 - e^{-\mu_t \pi}) \\ T_1 - T_2 &= T_1(1 - e^{-\mu_t \pi}) \\ T_a - T_1 &= T_a(1 - e^{-\mu_s \theta_s}) \end{aligned} \tag{4}$$

where, μ_t and μ_s are the friction coefficients of the Teflon tube and the Bowden cable, respectively; the θ_s is the curvature angle of the Bowden cable. Using the given equation, the final tension distribution can be obtained as

$$\begin{aligned} T_1 &= T_M e^{-\mu_s \theta_s} \\ T_2 &= T_M e^{-\mu_s \theta_s - \mu_t \pi} \\ T_3 &= T_M e^{-\mu_s \theta_s - 2\mu_t \pi} \\ T_4 &= T_M e^{-\mu_s \theta_s - 3\mu_t \pi}. \end{aligned} \tag{5}$$

We can see that the tension of the tendon gradually decreases as the tendon goes from segment 1 to segment 4. When the exact value of the friction coefficient is used in the above equations, the tension distribution of TR1 can be summarized as shown in Table.I. An overall comparison with the other tendon routings (TR1 - TR7) is provided in Fig. 9.

C. Tension distribution of tendon routing 2

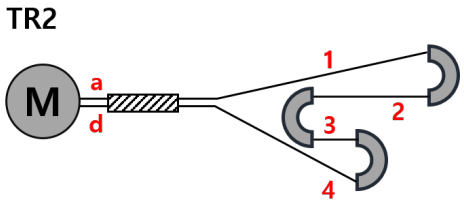

Fig. 3. **Schematic of tendon routing 2**
Tendon routing 2 (TR2) schematic to derive the tension distribution.

TABLE II
TENSION DISTRIBUTION OF TENDON ROUTING 2

	T_M	T_1	T_2	T_3	T_4
TR1	1	0.21	0.12	0.07	0.12
Ratio	-	41(%)	23(%)	13(%)	23(%)

In TR2 (Fig. 3), both sides of the tendon are fixed at the motor. In this case, the tension distribution is more uniform than in the TR1 case because each side of the tendon (segment 1 and 4) is pulled by the tendon at segments a and d, respectively. Here, the force relationship between each of the segments can be described as

$$\begin{aligned} T_M &= T_a + T_d \\ T_a - T_1 &= T_a(1 - e^{-\mu_s \theta_s}) \\ T_d - T_4 &= T_d(1 - e^{-\mu_s \theta_s}) \\ T_1 - T_2 &= T_1(1 - e^{-\mu_t \pi}) \\ T_2 - T_3 &= T_2(1 - e^{-\mu_t \pi}) \\ T_4 - T_3 &< T_4(1 - e^{-\mu_{t,s} \pi}). \end{aligned} \tag{6}$$

Here, the tendon between segments 3 and 4 does not move theoretically. Therefore, the exact friction between segments 3 and 4 cannot be defined and the only information about the friction is that the friction is less than the maximum static frictional force. However, when the tendon elongates when the tension increases, the friction between segments 3 and 4 can be defined as kinetic friction. Therefore, the relationship between T_3 and T_4 can be defined as

$$T_4 - T_3 = T_4(1 - e^{-\mu_t \pi}). \tag{7}$$

Using the force relationship shown in Eq (6) - Eq (7), the final tension distribution can be obtained as

$$\begin{aligned} T_1 &= K_{tr2} T_M e^{-\mu_s \theta_s} \\ T_2 &= K_{tr2} T_M e^{-\mu_s \theta_s - \mu_t \pi} \\ T_3 &= K_{tr2} T_M e^{-\mu_s \theta_s - 2\mu_t \pi} \\ T_4 &= K_{tr2} T_M e^{-\mu_s \theta_s - \mu_t \pi} \end{aligned} \tag{8}$$

where, K_{tr2} is gain, to simplify the tension distribution. The mathematical expression of K_{tr2} can be represented as

$$K_{tr2} = (1 + e^{-\mu_t \pi})^{-1}. \tag{9}$$

Here, the tension decreases from segment 1 to segment 3; however, the tension at tendon segment 4 is larger than that of the tendon at segment 3 because the tendon of segment 4 is directly pulled by the motor by being pulled through segment a. When the exact value of the friction coefficient is used in the above equations, the tension distribution of TR2 can be summarized as shown in Table.II.

D. Tension distribution of tendon routing 3

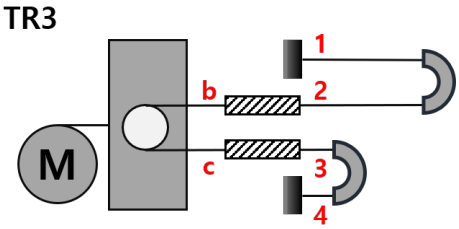

Fig. 4. **Schematic of tendon routing 3**
Tendon routing 3 (TR3) schematic to derive the tension distribution.

In TR3 (Fig. 4), both sides of the tendon are fixed at the end-effector and the tension is applied by pulling a movable pulley that is located at the middle of the tendon. Since a movable pulley is used, friction between segment

TABLE III

TENSION DISTRIBUTION OF TENDON ROUTING 3

TR3	T_M	T_1	T_2	T_3	T_4
	1	0.09	0.16	0.16	0.09
Ratio	-	18(%)	32(%)	32(%)	18(%)

b and segment c is defined by the rolling friction of the bearing; the rolling friction coefficient is represented as μ_b in this paper. Here, the friction between segment 2 and segment b is not defined because the tendon at segment 1 and segment 2 does not move. However, by considering the tendon elongation, the friction between segment 2 and segment b is also considered as a kinetic friction. With the above assumption, the relationship of the tension in each segment can be described as

$$\begin{aligned} T_M &= T_b + T_c \\ T_b - T_2 &= T_b(1 - e^{-\mu_s \theta_s}) \\ T_2 - T_1 &= T_2(1 - e^{-\mu_t \pi}) \\ T_b - T_c &= T_b(1 - e^{-\mu_b \pi}) \\ T_c - T_3 &= T_c(1 - e^{-\mu_s \theta_s}) \\ T_3 - T_4 &= T_3(1 - e^{-\mu_t \pi}). \end{aligned} \tag{10}$$

Similar to other cases, the final tension distribution was obtained as

$$\begin{aligned} T_1 &= T_M K_{tr3} e^{-\mu_s \theta_s - \mu_t \pi} \\ T_2 &= T_M K_{tr3} e^{-\mu_s \theta_s} \\ T_3 &= T_M K_{tr3} e^{-\mu_b \pi - \mu_s \theta_s} \\ T_4 &= T_M K_{tr3} e^{-\mu_b \pi - \mu_s \theta_s - \mu_t \pi} \end{aligned} \tag{11}$$

where, K_{tr3} is the variable used for simplification; the explicit form of K_{tr3} can be described as

$$K_{tr3} = (1 + e^{-\mu_b \pi})^{-1}. \tag{12}$$

In this routing, thanks to tendon elongation, the difference of the tensions at segment 2 and segment 3 do not differ significantly from the tension differences at segment b and segment c, even when the friction of the Bowden cable is considered. When the exact value of the friction coefficient is used in the above equations, the tension distribution of TR3 can be summarized as shown in Table.III.

E. Tension distribution of tendon routing 4

TABLE IV

TENSION DISTRIBUTION OF TENDON ROUTING 4

TR4	T_M	T_1	T_2	T_3	T_4
	1	0.29	0.16	0.05	0.03
Ratio	-	54(%)	31(%)	10(%)	6(%)

In TR4 (Fig. 5), one side of the tendon is fixed at the end-effector, while the other side of tendon is fixed at the

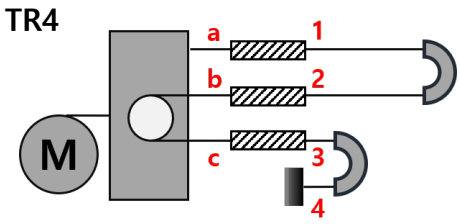

Fig. 5. **Schematic of tendon routing 4**
Tendon routing 4 (TR4) schematic to derive the tension distribution.

motor. Also, the movable pulley is used between segment b and segment c to apply kinetic constraints at the two fingers.

In this case, tension distribution can be obtained because the moving direction of the tendon is straightforward. Here, when the motor pulls the tendon, the tendon passes from segment 4 to segment 1 and finally it is pulled to segment a. Therefore, the force equations of the tension can be described as

$$\begin{aligned} T_M &= T_a + T_b + T_c \\ T_a - T_1 &= T_a(1 - e^{-\mu_s \theta_s}) \\ T_1 - T_2 &= T_1(1 - e^{-\mu_t \pi}) \\ T_2 - T_b &= T_2(1 - e^{-\mu_s \theta_s}) \\ T_b - T_c &= T_b(1 - e^{-\mu_b \pi}) \\ T_c - T_3 &= T_c(1 - e^{-\mu_s \theta}) \\ T_3 - T_4 &= T_3(1 - e^{-\mu_s \pi}) \end{aligned} \tag{13}$$

Accordingly, the final tension distribution can be obtained as

$$\begin{aligned} T_1 &= K_{tr4} T_M e^{-\mu_s \theta_s} \\ T_2 &= K_{tr4} T_M e^{-\mu_s \theta_s - \mu_t \pi} \\ T_3 &= K_{tr4} T_M e^{-3\mu_s \theta_s - \mu_t \pi - \mu_b \pi} \\ T_4 &= K_{tr4} T_M e^{-3\mu_s \theta_s - 2\mu_t \pi - \mu_b \pi} \end{aligned} \tag{14}$$

where, K_{tr4} is the variable for the simplification, which is described as

$$K_{tr4} = (1 + e^{-2\mu_s \theta_s - \mu_t \pi} + e^{-2\mu_s \theta_s - \mu_t \pi - \mu_b \pi})^{-1}. \tag{15}$$

In TR3, the tension difference between segment 2 and segment 3 is small, while in TR4 the tension difference between these two segments is large. This is caused by the difference in the direction of the tendon movement in both paths. − In TR3, the tendon moves in the direction pulled into segments b and c in segments 2 and 3. In TR4, on the other hand, the tendon moves in the direction from segment 3 to segment c and from segment b to segment 2. When the exact value of the friction coefficient is used in the above equations, the tension distribution of TR4 can be summarized as shown in Table.IV.

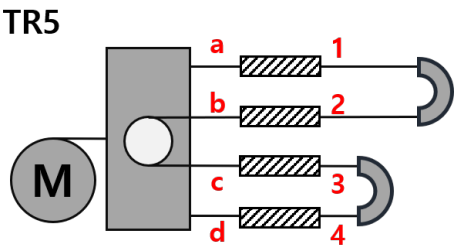

Fig. 6. **Schematic of tendon routing 5**
Tendon routing 5 (TR5) schematic to derive the tension distribution.

TABLE V
TENSION DISTRIBUTION OF TENDON ROUTING 5

TR5	T_M	T_1	T_2	T_3	T_4
	1	0.18	0.10	0.03	0.02
Ratio	-	54(%)	31(%)	10(%)	6(%)

F. Tension distribution of tendon routing 5

In TR5 (Fig. 6), both sides of the tendon are fixed at the motor and the kinetic constraint is also applied by a movable pulley that is installed at the motor. Here, the tendon moves in a way that is similar to the motion of the tendon in TR4. In this tendon routing, the force equations of the tension can be obtained as

$$\begin{aligned} T_M &= T_a + T_b + T_c + T_d \\ T_a - T_1 &= T_a(1 - e^{-\mu_s \theta_s}) \\ T_1 - T_2 &= T_1(1 - e^{-\mu_t \pi}) \\ T_2 - T_b &= T_2(1 - e^{-\mu_s \theta_s}) \\ T_b - T_c &= T_b(1 - e^{-\mu_b \pi}) \\ T_c - T_3 &= T_c(1 - e^{-\mu_s \theta_s}) \\ T_3 - T_4 &= T_3(1 - e^{-\mu_t \pi}) \\ T_4 - T_d &= T_4(1 - e^{-\mu_s \theta_s}) \end{aligned} \tag{16}$$

Further, the final tension distribution can be obtained as

$$\begin{aligned} T_1 &= K_{tr5} T_M e^{-\mu_s \theta_s} \\ T_2 &= K_{tr5} T_M e^{-\mu_s \theta_s - \mu_t \pi} \\ T_3 &= K_{tr5} T_M e^{-3\mu_s \theta_s - \mu_t \pi - \mu_b \pi} \\ T_4 &= K_{tr5} T_M e^{-3\mu_s \theta_s - 2\mu_t \pi - \mu_b \pi} \end{aligned} \tag{17}$$

where, K_{tr5} is

$$K_{tr5} = (1 + e^{-2\mu_s \theta_s - \mu_t \pi}(1 + e^{-\mu_b \pi} + e^{-\mu_t \pi - \mu_b \pi}))^{-1}. \tag{18}$$

Since the direction of the tendon in this tendon routing is similar to that of the tendon in TR4, the tension distribution is similar to that of TR4. The only difference is K_{tr5}, because this tendon routing pulls more tendon than in TR4. Here, we can infer that the tendon at segment a or segment d increases the difference in tension between segment 2 and segment 3; the tendon at segment a or segment d roles to apply kinematic constraints on the tendon and is forced to move the tendon. When the exact value of the friction coefficient is used in the above equations, the tension distribution of TR5 can be summarized as shown in Table.V.

G. Tension distribution of tendon routing 6

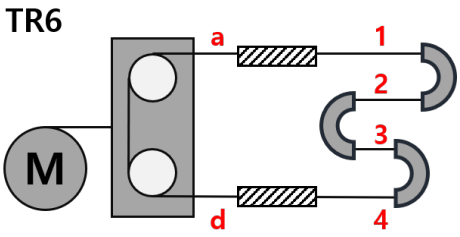

Fig. 7. **Schematic of tendon routing 6**
Tendon routing 6 (TR6) schematic to derive the tension distribution.

TABLE VI
TENSION DISTRIBUTION OF TENDON ROUTING 6

TR6	T_M	T_1	T_2	T_3	T_4
	1	0.16	0.09	0.09	0.16
Ratio	-	32(%)	18(%)	18(%)	32(%)

In TR6 (Fig. 7), neither side of the tendon has a fixation point. This tendon routing requires connections at both ends of the tendon. These connections sometimes can cause a problem in practical applications. This tendon routing makes two kinetic constraints by using both a movable pulley and a fixed pulley. The results of TR6 can be compared with the results of TR2 and TR3. We can say that TR2 applies kinematic constraints between the tendon at segment 1 and segment 4, while TR6 applies kinetic constraints between the tendon at segment 1 and segment 4.

The difference of constraints makes a big difference in the tension distribution because kinetic constraints make tendons in two segments have the same force, while kinematic constraints cause the tendons in two segments to move the same distance. In TR6, the force equations of the tension can be described as

$$\begin{aligned} T_M &= T_a + T_d \\ T_1 - T_2 &= T_1(1 - e^{-\mu_t \pi}) \\ T_2 - T_3 &< T_2(1 - e^{-\mu_{t,s} \pi}) \\ T_4 - T_3 &= T_4(1 - e^{-\mu_t \pi}) \\ T_4 - T_3 &= T_4(1 - e^{-\mu_t \pi}) \\ T_a - T_1 &= T_a(1 - e^{-\mu_s \theta_s}) \\ T_d - T_4 &= T_d(1 - e^{-\mu_s \theta_s}) \\ T_a - T_d &= T_a(1 - e^{-\mu_b \theta_b}) \end{aligned} \tag{19}$$

where, $\mu_{t,s}$ is the static friction coefficient of the Teflon tube. In these force equations, unlike other tendon routings, the relationship between the tension at segment 2 and the tension

at segment 3 is defined by static friction. This is because we cannot guarantee tendon movement even with an assumption about tendon elongation; if the tensions on both sides of the Teflon tube are exactly the same, they may extend in both directions from the center of the Teflon tube. Therefore, we cannot figure out the friction at this Teflon tube. Since both sides of the tension are the same, we assumed that the friction does not exist in this case. Using this assumption, the final tension distribution was obtained as

$$\begin{aligned} T_1 &= T_M K_{tr6} e^{-\mu_s \theta_s} \\ T_2 &= T_M K_{tr6} e^{-\mu_s \theta_s - \mu_t \pi} \\ T_3 &= T_M K_{tr6} e^{-\mu_b \pi - \mu_s \theta_s - \mu_t \pi} \\ T_4 &= T_M K_{tr6} e^{-\mu_s \theta_s - \mu_b \pi} \end{aligned} \tag{20}$$

where, K_{tr6} is the variable for simplification, which is expressed as

$$K_{tr6} = (1 + e^{-\mu_b \pi})^{-1}. \tag{21}$$

The tension distribution of TR6 is the same as that of TR3. This is because the friction between segment 2 and segment 3 is assumed as zero in this tendon routing, as described above; the actual tension distribution is described in Table.VI.

H. Tension distribution of tendon routing 7

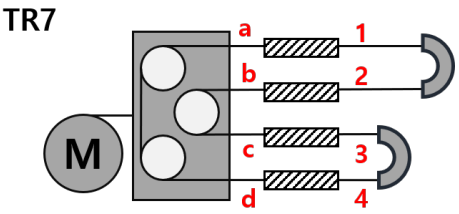

Fig. 8. **Schematic of tendon routing 7**
Tendon routing 7 (TR7) schematic to derive the tension distribution.

TABLE VII
TENSION DISTRIBUTION OF TENDON ROUTING 7

TR7	T_M	T_1	T_2	T_3	T_4
	1	0.32	0.32	0.32	0.32
Ratio	-	25(%)	25(%)	25(%)	25(%)

In TR7 (Fig. 8), as in TR6, both ends of the tendon are connected to each other. In this case, there are two kinetic constraints between segment a and segment d or between segment b and segment c. Since movable pulleys are used, the friction of the tendon between segment a and segment d, and friction between segment b and segment c can be obtained. Here, the situation in the Teflon tube between segment 1 and segment 2 or segment 3 and segment 4 is similar to the situation in the Teflon tube between segments 2 and 3 of TR6. Therefore, the force equations of the tension can be described as

$$\begin{aligned} T_M &= T_a + T_b + T_c + T_d \\ T_3 - T_4 &< T_3(1 - e^{-\mu_t \pi}) \\ T_1 - T_2 &< T_1(1 - e^{-\mu_t \pi}) \\ T_a - T_1 &= T_a(1 - e^{-\mu_s \theta_s}) \\ T_b - T_2 &= T_b(1 - e^{-\mu_s \theta_s}) \\ T_c - T_3 &= T_c(1 - e^{-\mu_s \theta_s}) \\ T_d - T_4 &= T_d(1 - e^{-\mu_s \theta_s}) \\ T_a - T_d &= T_a(1 - e^{-\mu_b \pi}) \\ T_b - T_c &= T_b(1 - e^{-\mu_b \pi}) \end{aligned} \tag{22}$$

Finally, the tension distribution can be expressed as

$$\begin{aligned} T_1 &= K_{tr7} T_M e^{-\mu_s \theta_s} \\ T_2 &= K_{tr7} T_M e^{-\mu_s \theta_s} \\ T_3 &= K_{tr7} T_M e^{-\mu_s \theta_s - \mu_b \pi} \\ T_4 &= K_{tr7} T_M e^{-\mu_s \theta_s - \mu_b \pi} \end{aligned} \tag{23}$$

where, K_{tr7} is

$$K_{tr7} = 0.5(1 + e^{-\mu_b \pi})^{-1}. \tag{24}$$

We can see that the tension distribution of TR7 is relatively uniform, as compared with the other tendon routings. Here, we assumed that there is no tendon movement between segments 3 and 4 and between segments 1 and 2, similar to the case of TR6. When the exact value of the friction coefficient is used in the above equations, the tension distribution of TR7 can be summarized as shown in Table.VII. Since it is not straightforward, we verified the simulation results by comparing the results with the experimental results. The comparison between the modeling results and the experimental results is described in the next section. Fortunately, friction between segment 1 and segment 2 and friction between segment 3 and segment 4 were negligible in the experiment; this is explained in Figure 9.

I. Conclusion

The simulated results shown in Table I - Table VII can be summarized and can be compared with the experimental results shown in Fig. 9. Here, the line + symbol graph depicts the simulation results, while the bar graph shows the experimental results. All simulation results were normalized so that the sum of T1 and T4 is equal to 1. As can be seen from the figure, the tension distributions of the seven tendon routings obtained through simulation and experimentation show similar tendencies. When the friction coefficient between the Teflon tube and the tendon is 0.18, which is a value obtained in previous research, the rms error between the experimental and simulation results is 13.6%. However, rms error can be minimized to 3.4% by setting the friction coefficient to 0.09. The smaller friction measured than that measured in the previous research is inferred by the effect of the spring, which is used to prevent deformation of the Teflon tube. In the previous study, force measurements

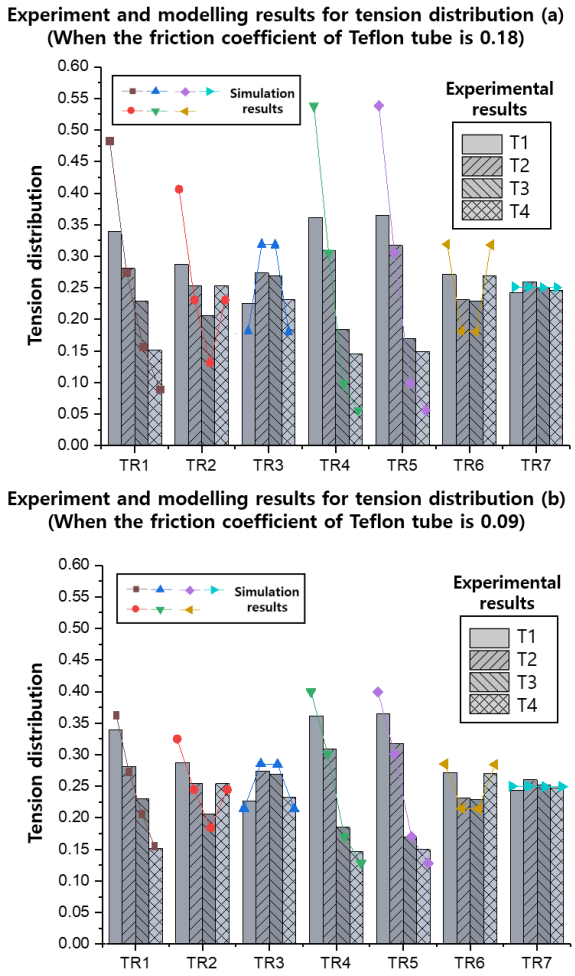

Fig. 9. **Tension distributions of the seven different tendon routings** The bar graph shows the experimental results of the tension distribution in each of the tendon routings, while the line+symbol graph in the figure shows the simulation results. **(a)** shows the simulation results with the friction coefficient of 0.18 and **(b)** shows the simulation results with the friction coefficient of 0.09.

were done without preventing the deformation of the Teflon tube; whereas, in this study, the surface of the Teflon tube was wrapped with a spring to minimize deformation of the Teflon tube. It is true that using springs could be an unfair measurement because the springs are not used in the actual wearable robot application. Nevertheless, we used the springs for more reliable data acquisition. In fact, neither value (i.e., 0.09 and 0.18) is a problem because the values are within the range shown in the literature; the literature value of the friction coefficient between a Teflon tube and steel is known to be 0.05 - 0.2. Since the results of the simulation and experiment show similar trends, we conclude that the proposed simulation method is suitable to use without the need for laborious experiments.

REFERENCES

[1] M. Kaneko, M. Wada, H. Maekawa, and K. Tanie, "A new consideration on tendon-tension control system of robot hands," *Proceedings. 1991 IEEE International Conference on Robotics and Automation IEEE International Conference on Robotics and Automation, Sacramento, California, USA,*, pp. 1028–1033, 1991.

[2] H. In, B. B. Kang, M. Sin, and K.-J. Cho, "Exo-glove: A wearable robot for the hand with a soft tendon routing system," *IEEE Robotics & Automation Magazine*, vol. 22, no. 1, pp. 97–105, 2015.